Journal of Materials Chemistry C

ROYAL SOCIETY OF CHEMISTRY

PAPER

View Article Online
View Journal | View Issue

Cite this: J. Mater. Chem. C, 2021, 9, 15868

Epitaxial growth of β-Ga_2O_3 (−201) thin film on four-fold symmetry CeO_2 (001) substrate for heterogeneous integrations†

Xiao Tang,*[a] Kuang-Hui Li,[a] Che-Hao Liao,[a] Dongxing Zheng,[b] Chen Liu,[b] Rongyu Lin,[a] Na Xiao,[a] Shibin Krishna,[a] Jose Tauboada[a] and Xiaohang Li*[a]

β-Ga_2O_3 is a wide bandgap semiconductor material that is promising for many fields such as gas sensors, UV detectors, and high-power electronics. Until now, most epitaxial β-Ga_2O_3 thin films could only be realized on six-fold symmetric single crystal substrates including sapphire (0001), 3C-SiC (001), and native β-Ga_2O_3. In this report, we demonstrate the epitaxial growth of β-Ga_2O_3 (−201) thin films on non-six-fold symmetric substrates, *i.e.*, the CeO_2 (001) substrate. Different from the conventional six-fold symmetric sapphire substrates, the four-fold symmetric cubic phase CeO_2 (001) induces the formation of two sets of hexagonal-like atom frameworks with a mutual rotation angle of 90° in the β-Ga_2O_3 (−201) plane. This is due to the small lattice mismatch between the β-Ga_2O_3 (−201) plane and the CeO_2 (001) plane in two directions: CeO_2 [100]//β-Ga_2O_3 [010] and CeO_2 [010]//β-Ga_2O_3 [010]. Besides, the valence band offset (VBO) and the conduction band offset (CBO) at the β-Ga_2O_3/CeO_2 heterojunction are examined using high-resolution X-ray photoelectron spectroscopy (HR-XPS) and are estimated to be 1.63 eV and 0.18 eV, respectively, suggesting a type-II heterostructure. The obtained epitaxial β-Ga_2O_3 thin films are fabricated into photodetectors (PDs), which show key photoelectrical characteristics that are similar to those of PDs using the conventional sapphire substrate. The results indicate the epitaxial β-Ga_2O_3 thin films on CeO_2 have a high crystallization quality, and thus are capable of producing various essential devices. Moreover, the epitaxy between β-Ga_2O_3 (−201) and CeO_2 (001) demonstrated in this work can pave the way for constructing heterostructures between β-Ga_2O_3 and other cubic-phase functional materials, such as p-type semiconductors, piezoelectric semiconductors, and superconductors.

Received 19th June 2021,
Accepted 19th September 2021

DOI: 10.1039/d1tc02852a

rsc.li/materials-c

Introduction

Over the past decade, Ga_2O_3 as a wide bandgap semiconductor material has attracted tremendous attention because of its potential applications, such as in gas sensors, UV photodetectors (PDs), and high-power electronics.[1–7] It is known that Ga_2O_3 has various types of crystalline structures, including α, β, γ, δ, and ε.[1] Compared with other crystal types, monoclinic β-Ga_2O_3 is considered as the most promising candidate since it has the highest thermal stability. β-Ga_2O_3 thin films ought to be deposited on substrates that have a smaller lattice mismatch than β-Ga_2O_3. Therefore, the most straightforward method to ensure the high quality of β-Ga_2O_3 thin films is the adoption of the homoepitaxial growth route using a β-Ga_2O_3 single crystal substrate due to a zero lattice-mismatch.[2] However, until now, β-Ga_2O_3 single-crystal substrates have not been cost-effective. As a compromise between the film quality and the cost, sapphire (α-Al_2O_3) (0001) and 3C-SiC (001) single-crystal substrates are more commonly used as the epitaxial templates for the growth of β-Ga_2O_3 thin films. Here, the sapphire (0001) and 3C-SiC (001) all have a six-fold in-plane symmetry. As a result, the obtained β-Ga_2O_3 thin films have a (−201) orientation that shows a hexagonal-like atom framework owing to the epitaxy relationship.[3,6]

On the other hand, as another group of the commonly used substrates, the four-fold symmetric (001) oriented cubic crystalline materials such as yttria-stabilized zirconia (YSZ), $SrTiO_3$, $LaAlO_3$, MgO, and CeO_2 have been widely used as epitaxial templates for various cubic-phase functional thin films.[8–12] However, to the best of our knowledge, investigation of the lattice adaptation of such substrates to β-Ga_2O_3(−201) is

[a] Advanced Semiconductor Laboratory, King Abdullah University of Science and Technology (KAUST), Thuwal 23955-6900, Saudi Arabia. E-mail: xiao.tang@kaust.edu.sa

[b] Division of Physical Science and Engineering (PSE), King Abdullah University of Science and Technology (KAUST), Thuwal 23955-6900, Saudi Arabia

† Electronic supplementary information (ESI) available. See DOI: 10.1039/d1tc02852a

rare.[4,13,14] On the use of cubic phase substrates, we notice that Wakabayashi *et al.* demonstrated the epitaxial growth of β-Ga_2O_3 (001) on MgO (001); around the same time, Nishinaka *et al.* demonstrated the epitaxial growth of β-Ga_2O_3 (−201) on YSZ (111) and MgO (111).[13,14] In all these cases, the thin-film growth obeys either a "four-fold on four-fold" or "six-fold on six-fold" epitaxial relationship. Nevertheless, the epitaxial relationship between the six-fold symmetric β-Ga_2O_3 (−201) orientation and the four-fold symmetric (001) cubic planes has not been reported. For the (−201) oriented β-Ga_2O_3 thin films, they can be easily combined with other hexagonal wide bandgap (WBG) semiconductor materials, such as GaN, AlN, and SiC, to make transistors and power devices.[6,15,16] For the (001) oriented cubic materials, the (001) plane is not only the cleavage and the most straightforwardly acquired facet, but also offers various unique performance features compared with the other oriented plane. Thus, constructing the epitaxy relationship between the β-Ga_2O_3 (−201) plane and the cubic (001) plane can provide the possibility of creating various functional heterojunctions and pave the way for combining cubic functional materials and other WBG semiconductor family member materials.[17,18] More importantly, nowadays, epitaxial cubic phase (001) thin films including MgO and CeO_2 can be routinely grown using the ion-beam-assisted deposited (IBAD) technique on polycrystalline flexible substrates, and these have been widely applied in the fields of producing coated conductors.[19,20] Therefore, constructing such an epitaxy relationship is also important for adopting the IBAD technique in the fabrication of flexible hexagonal semiconductor devices.

In this work, we demonstrate the epitaxial growth of β-Ga_2O_3 thin films *via* pulsed laser deposition (PLD) on the CeO_2 (001) substrate. Here, the CeO_2 layer has a fluorite structure that crystallizes in the cubic $Fm\bar{3}m$ space group, therefore showing a four-fold symmetric crystallinity. The X-ray diffraction (XRD) 2-theta scan indicates that the deposited Ga_2O_3 thin film has a beta-phase with a preferred orientation along [201]. The in-plane epitaxial relationship between the CeO_2 (001) plane and the β-Ga_2O_3 (−201) plane is investigated using pole figure measurements. The results reveal the formation of two sets of hexagonal-like atom frameworks with a mutual rotation angle of 90° in the β-Ga_2O_3 (−201) plane. Besides, the valence band offset (VBO) and the conduction band offset (CBO) at the β-Ga_2O_3/CeO_2 heterojunction are examined using high-resolution X-ray photoelectron spectroscopy (HR-XPS) and are estimated to be 1.63 eV and 0.18 eV, respectively, suggesting a type-II heterostructure. To evaluate the quality of the epitaxial β-Ga_2O_3 thin films using CeO_2 (001) substrates, the samples are fabricated into PDs. For comparison, Ga_2O_3 thin films are also deposited using the conventional sapphire and polycrystalline silicon (p-Si) substrates and fabricated into PDs as well. The photoelectrical characteristics of the PDs based on the β-Ga_2O_3/CeO_2 heterojunction are found to be similar to those based on the β-Ga_2O_3/sapphire heterojunction and are significantly superior to those based on the β-Ga_2O_3/p-Si heterojunction. The results indicate that the epitaxial β-Ga_2O_3 thin films on CeO_2 have a high crystallization quality and thus are capable of producing various semiconductor devices. The epitaxy between β-Ga_2O_3 (−201) and CeO_2 (001) that is demonstrated in this work may also pave the way for constructing heterostructures between β-Ga_2O_3 and various other cubic-phase functional materials, such as p-type semiconductors (*e.g.*, NiO), superconductors (*e.g.*, $YBa_2Cu_3O_{7-x}$, $Ba_{0.6}K_{0.4}BiO_3$, and PtSbS), and piezoelectric semiconductors (*e.g.*, $PbZrO_3$, $BaTiO_3$, and $PbNiO_3$).[21–28]

Experimental section

The β-Ga_2O_3 thin films were deposited using the PLD technique on CeO_2 (001)-coated YSZ substrates from the MTI Corporation. During the deposition process, the β-Ga_2O_3 target was irradiated using a KrF excimer laser (248 nm wavelength) of 300 mJ for 25 000 pulses at a frequency of 5 Hz. The working distance was set at 95 mm. The temperature and the oxygen partial pressure were set at 640 °C and 5 mTorr, respectively. The Ga_2O_3 thin films were also deposited on sapphire (0001) and p-Si substrates as the reference samples in the PLD system using the same parameters. The PDs were fabricated by depositing the β-Ga_2O_3 thin films using magnetron sputter deposition to form Ohmic contacts. The spacing between the PD fingers was kept at 30 μm.

The $2\theta - \omega$ XRD scan, rocking curve, and pole figures were obtained using a Bruker D8 Ultra XRD system. Atomic force microscopy (AFM) measurements were carried out using a CSI Instruments Nano-Observer system. The study of the film surface morphology and the preparation of the high-resolution transmission electron microscopy (HR-TEM) lamella of the heterostructures of β-Ga_2O_3/CeO_2/YSZ were performed using an FEI Helios G4 dual-beam focused ion beam scanning electron microscope system. The HR-TEM images and fast Fourier transform (FFT) patterns of the β-Ga_2O_3/CeO_2/YSZ interfaces were obtained using an HR-TEM system (Titan ST microscope; FEI, USA) with an operating voltage of 300 keV. For the high-resolution HR-XPS measurements, the signals were recorded using a Kratos Axis Ultra DLD spectrometer equipped with a monochromatic Al Ka X-ray source ($h\nu$ = 1486.6 eV) at 150 W. The base pressure during the measurements was maintained under 10^{-9} mbar. The binding energy of C 1s = 284.8 eV was taken as a reference. Ultraviolet–visible spectroscopy (UV/Vis) measurements were performed using a LAMBDA 950 UV/Vis/NIR spectrophotometer from PerkinElmer. The photoelectrical characteristics were measured using a Zolix DSR600-X150-200-UV automated spectro-radiometric measurement system, with an illumination power density of 20 μW cm^{-2}.

Results and discussion

To evaluate the phase purity and the crystallinity of the grown Ga_2O_3 thin films, $2\theta - \omega$ XRD scans were carried out on the β-Ga_2O_3 thin films deposited on the CeO_2/YSZ substrate, as well as those deposited on sapphire and p-Si substrates as the reference samples. The stacked $2\theta - \omega$ XRD scans are shown in Fig. 1(a). For the sample using the CeO_2/YSZ substrate, the peaks at 18.5°, 37.8°, and 58.6° from diffractions of the (−201),

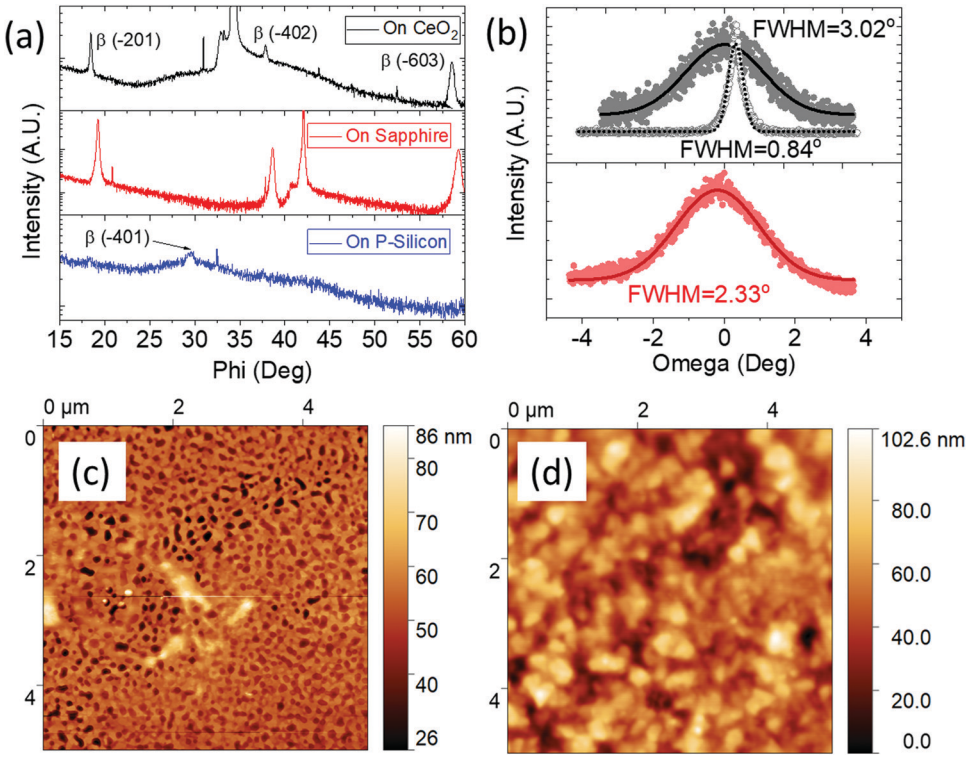

Fig. 1 (a) $2\theta - \omega$ XRD spectra of β-Ga_2O_3 thin films on the sapphire, CeO_2/YSZ, and p-Si substrates; (b) the rocking curve of β-Ga_2O_3 (−201) using CeO_2 substrate (solid gray), the rocking curve of CeO_2 (002) (empty gray), and the rocking curve of β-Ga_2O_3 (−201) using sapphire substrate (solid red); (c) the AFM image of the CeO_2/YSZ substrate; and (d) the AFM image of the β-Ga_2O_3 thin films.

(−402), and (−603) planes of β-Ga_2O_3 are the same as for the sample using the conventional sapphire substrate, except for the peaks at 32.8° and 34.4°, which correspond to diffractions from the (002) plane of CeO_2 and YSZ, respectively. First, the XRD spectra show no peaks potentially from the Ga–Ce–O ternary compound induced by the diffusion of cerium during the high-temperature deposition process, indicating a high phase purity of β-Ga_2O_3. Second, the absence of the (−401) peak at around 30°, which corresponds to the random orientations of β-Ga_2O_3, in the XRD spectra indicates the good crystallinity of the grown β-Ga_2O_3 thin films.[27] Despite the fundamental symmetry difference between CeO_2 (001) and the conventional hexagonal symmetric substrates, the observed single preferred orientation along [201] of the formed β-Ga_2O_3 thin films is the same as that deposited on the sapphire substrate.[29–31] By contrast, the thin films using the p-Si substrate show a polycrystalline structure, as evidenced from the appearance of the (−401) peak located at 30°. The grain size could be estimated according to the Scherrer formula (1):

$$D = \frac{K\lambda}{\mathrm{FWHM}\cos t\theta} \quad (1)$$

where D represents the grain size (nm) along the normal direction of the diffraction planes, K is taken as 1, λ represents the wavelength of the X-ray (nm) and is 1.54 Å, and θ is the diffraction angle. The grain size of the samples deposited on the CeO_2/YSZ and sapphire substrates are calculated as 49.5 nm and 45.5 nm, respectively. For the sample on p-Si, the size was not calculated for comparison since the grains are randomly oriented. The rocking curve was also measured on the β-Ga_2O_3 (−201) peak for the samples using the CeO_2/YSZ and sapphire substrates, as shown in Fig. 1(b). The full width at half maximum (FWHM) value of β-Ga_2O_3 (−201) on the CeO_2/YSZ and sapphire substrates was estimated as 3.02° and 2.33°, respectively. Also, the rocking curve was measured on the CeO_2 (002) and gives an FWHM value of 0.84°, as shown in Fig. 1(b); however, the conventional sapphire substrate has a FWHM value of 100–200 arcsec (not shown in the image for its ultra-low FWHM value). Compared with the huge crystal difference between sapphire and CeO_2, the slight increase in the FWHM value of β-Ga_2O_3 from using sapphire to using CeO_2 suggests a good epitaxy ability of CeO_2 (001) for growing high-quality β-Ga_2O_3 (−201) thin films.[32] Fig. 1(c and d) show the AFM images of the CeO_2 (001)-coated YSZ substrates and the β-Ga_2O_3 thin films, respectively. Upon deposition of the β-Ga_2O_3 thin films, large grains can be clearly seen on the surface, making the RMS surface roughness increase from 3.96 nm to 7.51 nm.

To investigate the epitaxial relationship between the β-Ga_2O_3 (−201) plane and the CeO_2 (001) plane at the interface, a pole figure is obtained for the β-Ga_2O_3 thin film sample. Fig. 2(a) represents the pole figure composed of signals from the CeO_2 (111) and β-Ga_2O_3 (−401) planes. The CeO_2 (001) plane exhibits four intense in-plane CeO_2 (111) poles centered at Psi = 55.0° when the 2-theta angle is set at 28.5°, indicating the typical four-fold symmetry of the cubic crystal structure. It is known that β-Ga_2O_3 has monoclinic unit cells, which have two-fold

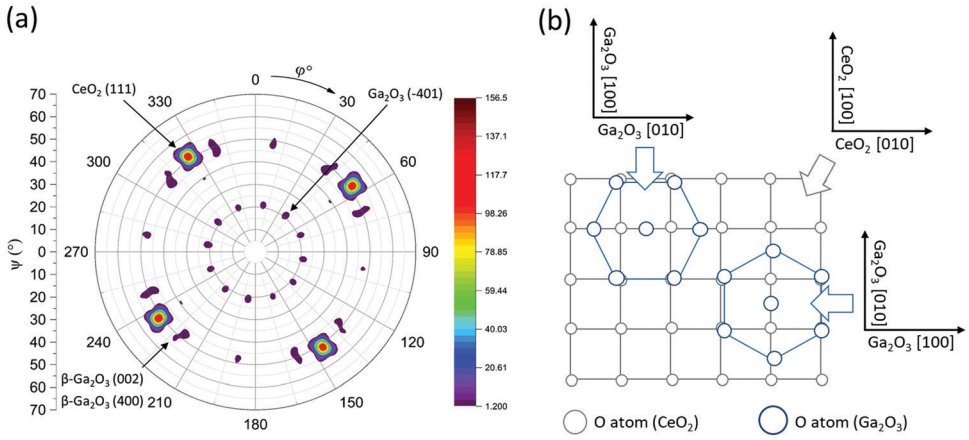

Fig. 2 (a) Pole figures recorded on β-Ga_2O_3 thin films deposited on the CeO_2 (001)-coated YSZ substrate, where the 2θ values are equal to 28.5° and 30.4° for CeO_2 (111) and β-Ga_2O_3 (−401), respectively; and (b) schematic of the epitaxial relationship between the CeO_2 (001) plane and the β-Ga_2O_3 (−201) plane.

symmetry. However, within the (−201) plane, either gallium or oxygen atoms are distributed in an irregular "hexagonal-like" configuration.[33–35] Hence, six in-plane β-Ga_2O_3 (−401) poles should be observed due to the six-fold symmetry. However, the results show twelve poles centered at Psi = 22.0° when the 2-theta angle is set at 30.4°. This is conflicts with the phenomenon observed on the β-Ga_2O_3 thin films using sapphire substrates.[34] Besides, twelve weak symmetry poles are also observed at the same Psi and 2-theta angles of the CeO_2 (111) plane, and the same Phi angles of the β-Ga_2O_3 (−401) plane. Based on such information and the lattice parameters of β-Ga_2O_3 (a = 1.223 nm, b = 0.304 nm, c = 0.580 nm and β = 103.70°), the twelve peaks are attributed to either β-Ga_2O_3 (400) (2-theta = 30.06°, Psi = 53.81°) or β-Ga_2O_3 (002) (2-theta = 31.73°, Psi = 50.02°). First of all, the twelve-fold symmetry poles for β-Ga_2O_3 imply the formation of double hexagonal-like frameworks with a mutual phi-rotation angle of 90°. Second, the relative Phi-angle positions of the CeO_2 (111) poles to those of β-Ga_2O_3 (−401) poles suggest a rotation angle of 45° both clockwise and anti-clockwise between β-Ga_2O_3 [010] and CeO_2 [110]. Based on the above interpretation, the epitaxial relationship between the CeO_2 (001) plane and the Ga_2O_3 (−201) plane is depicted in Fig. 2(b). It is known that the distances between the neighboring oxygen atoms along the CeO_2 [100] and [010] directions are all 2.7 Å, while that for β-Ga_2O_3 [010] is 3.04 Å.[32,36] Therefore, the lattice mismatch between CeO_2 [100] (also [010]) and β-Ga_2O_3 [010] is calculated to be 10%, which is higher than that between the oxygen atoms in the β-Ga_2O_3 (−201) plane and the (001) c-plane sapphire.[4] However, the XRD measurements indicate that such a small lattice mismatch readily ensures the epitaxial growth of β-Ga_2O_3 (−201) thin films. The epitaxial relationship between them is determined as CeO_2 [001]//Ga_2O_3 [001] for out-of-plane orientation, and CeO_2 [100]//Ga_2O_3 [010] together with CeO_2 [010]//Ga_2O_3 [010] for in-plane orientation.

SEM and TEM images were obtained for the surface and the cross-section of the β-Ga_2O_3/CeO_2/YSZ sample, as shown in Fig. 3(a) and (b), respectively. The TEM image reveals that the β-Ga_2O_3 thin film has a thickness of 400 nm. A magnified image is

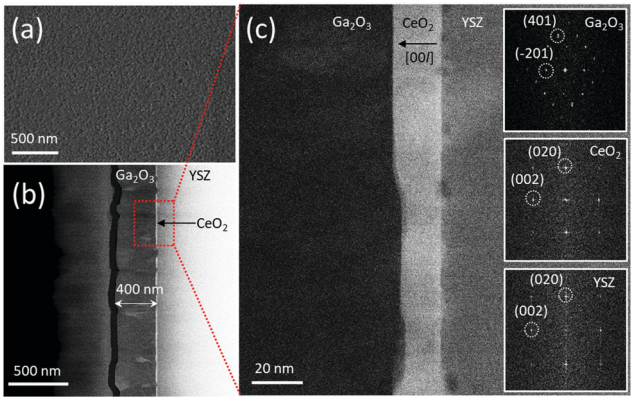

Fig. 3 (a) Scanning electron microscopy (SEM) image obtained on the surface of the β-Ga_2O_3 thin films; (b) the cross-sectional HR-TEM image acquired at the β-Ga_2O_3/CeO_2/YSZ interfaces; (c) the cross-sectional HR-TEM image acquired at the selected region of the β-Ga_2O_3/CeO_2/YSZ interfaces, together with the fast Fourier transform (FFT) patterns for individual layers of β-Ga_2O_3, CeO_2, and YSZ (the insets).

taken on the selected region, as shown in Fig. 3(c), and indicates a thickness of 20 nm for the CeO_2 layer. The fast Fourier transform (FFT) patterns for the individual layers of β-Ga_2O_3, CeO_2, and YSZ are shown in the insets of Fig. 3(c). The FFT patterns confirm the good crystalline quality of the β-Ga_2O_3 thin films and a plane spacing of 0.496 nm is determined for β-Ga_2O_3 (−201).

The band alignments of the β-Ga_2O_3/CeO_2 heterointerface are obtained using HR-XPS spectroscopy. The VBO (ΔE_V) and the CBO (ΔE_C) at the β-Ga_2O_3/CeO_2 heterointerface can be calculated *via* formula (2) and (3), respectively[25]

$$\Delta E_V = \left(E_{Ga2p}^{\beta\text{-}Ga_2O_3} - E_{VBM}^{\beta\text{-}Ga_2O_3}\right) - \left(E_{3d}^{CeO_2} - E_{VBM}^{CeO_2}\right) + \left(E_{Ce3d}^{\beta\text{-}Ga_2O_3/CeO_2} - E_{Ga2p}^{\beta\text{-}Ga_2O_3/CeO_2}\right) \quad (2)$$

$$\Delta E_C = \left(E_g^{CeO_2} - E_g^{\beta\text{-}Ga_2O_3}\right) - \Delta E_V \quad (3)$$

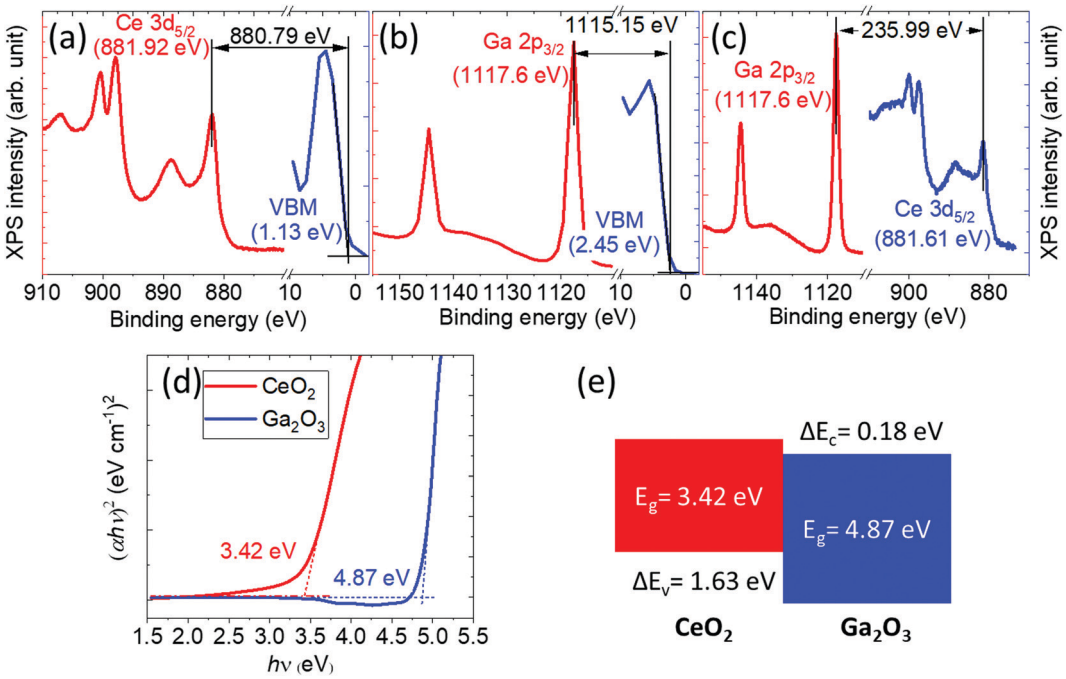

Fig. 4 (a) XPS spectra of the Ce 3d core levels and valence band from the CeO_2 layer; (b) XPS spectra of the Ga 2p core levels and valence band from the β-Ga_2O_3 layer; (c) XPS spectra of the Ce 3d and Ga 2p core levels from the β-Ga_2O_3/CeO_2 heterojunction; (d) Tauc plot of $(\alpha h\nu)^2$ as a function of the photon energy for the CeO_2 and the β-Ga_2O_3 thin films; and (e) schematic representation of the band alignment at the β-Ga_2O_3/CeO_2 heterointerface.

where $E_{Ga2p}^{\beta\text{-}Ga_2O_3}$, $E_{VBM}^{\beta\text{-}Ga_2O_3}$, $E_{3d}^{CeO_2}$, and $E_{VBM}^{CeO_2}$ are the core levels and the valence band maximum (VBM) for β-Ga_2O_3 and CeO_2, respectively; $E_{Ce3d}^{\beta\text{-}Ga_2O_3/CeO_2}$ and $E_{Ga2p}^{\beta\text{-}Ga_2O_3/CeO_2}$ are the corresponding values obtained on the β-Ga_2O_3/CeO_2 heterostructure; and $E_g^{CeO_2}$ and $E_g^{\beta\text{-}Ga_2O_3}$ are the optical band gaps of CeO_2 and β-Ga_2O_3, respectively. The core levels and the VBM are obtained from the XPS results, as shown in Fig. 4(a–c). For CeO_2, the binding energies of Ce $3d_{5/2}$ and the VBM are 881.92 eV and 1.13 eV, respectively; for β-Ga_2O_3, the binding energies of Ga $2p_{3/2}$ and the VBM are 1117.6 eV and 2.45 eV, respectively; and for the β-Ga_2O_3/CeO_2 heterostructure, the binding energies of Ce $3d_{5/2}$ and Ga $2p_{3/2}$ are determined as 881.61 eV and 1117.6 eV, respectively. By substituting these values into formula (2), the VBO value is calculated to be ΔE_V = 1.63 eV. The optical band gaps of CeO_2 and β-Ga_2O_3 are obtained from the UV–vis measurements and determined to be 3.42 eV and 4.87 eV, respectively (as shown in Fig. 4(d)). By substituting the calculated VBO (ΔE_V) and the optical band gap values of CeO_2 and β-Ga_2O_3 into formula (3), the CBO value at the β-Ga_2O_3/CeO_2 heterointerface is determined to be 0.18 eV. Based on the above calculations, the estimated band alignment diagram at the β-Ga_2O_3/CeO_2 heterointerface is illustrated in Fig. 4(e). The staggered gap suggests a type-II heterostructure between β-Ga_2O_3 and CeO_2.

To evaluate the quality of the epitaxial β-Ga_2O_3 thin films, the samples are fabricated into PDs by depositing Ti/Au contacts on the surface. A microscopic photograph taken on the surface of the β-Ga_2O_3 thin film PD during the AFM measurement is shown in Fig. 5(a). For comparison, Ga_2O_3 thin films grown on the sapphire and p-Si substrates are also fabricated into PDs using the same procedure. The *I–V* characteristics of the Ga_2O_3 thin film PDs grown on these three substrates under 250 nm illumination and without light are shown in Fig. 5(b). The photocurrent (I_P) at a bias of 5 V is maintained around the 10^{-7} A level and no significant difference can be observed in the same current scale for all three samples. In contrast, the three samples show an observable difference in the dark current (I_D), as $I_D^{Al_2O_3} < I_D^{CeO_2} < I_D^{Si}$. Responsivity, as a function of the illumination wavelength, is also measured on the PDs at a fixed bias of 5 V, as shown in Fig. 5(c). The responsivity is calculated using formula (4):

$$R = \frac{I_P - I_D}{P_\lambda S} \tag{4}$$

where I_P and I_D denote the photocurrent and the dark current, respectively, P_λ represents the illumination intensity and S represents the active area of the PDs. It can be clearly seen that the PDs deposited on the sapphire and CeO_2 substrates show a high responsivity in the DUV region ($R_{250\ nm}^{Al_2O_3} = 27$ A W^{-1}, $R_{250\ nm}^{CeO_2} = 18$ A W^{-1}) and a strong spectral selectivity ($R_{250\ nm}^{CeO_2} / R_{600\ nm}^{Al_2O_3} = 45.8$, $R_{250\ nm}^{CeO_2} / R_{600\ nm}^{CeO_2} = 30$). It is noted that two-dimensional Silvaco Atlas TCAD simulation was also carried out to examine the spectral response of 400-nm-thick Ga_2O_3 thin-film PDs grown on a 20 nm CeO_2 substrate, as shown in Fig. S1 (ESI†). The simulation results indicate that under the illumination of a power density of 20 μW cm^{-2}, the simulated spectral response is in good agreement with the actual experimental results. For the PD using the p-Si substrate, the

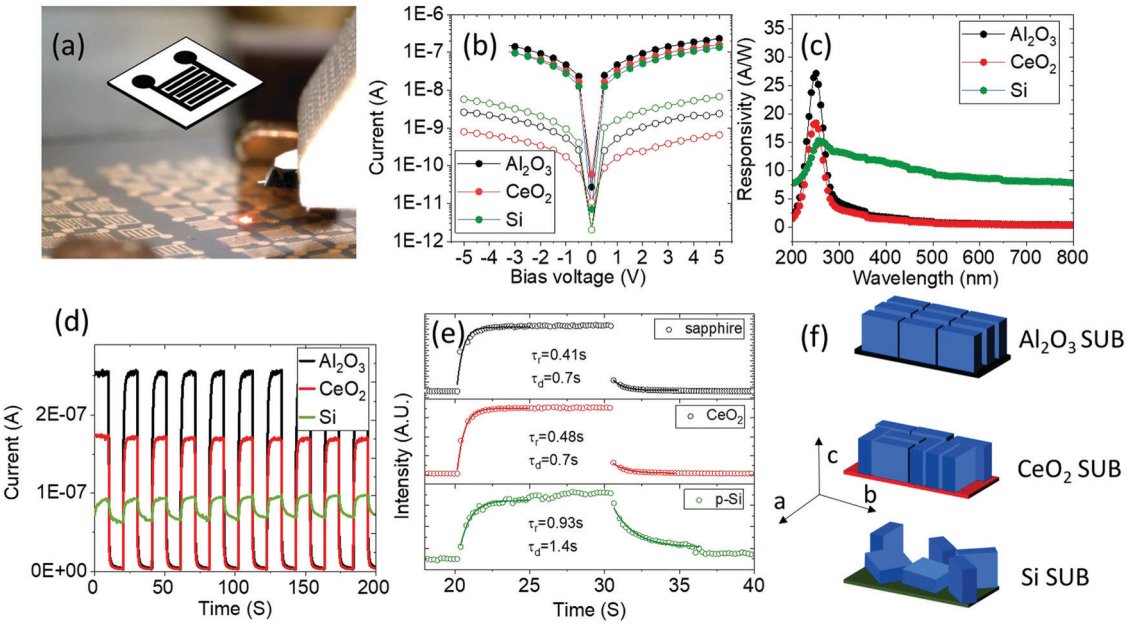

Fig. 5 (a) Microscopic photograph taken on the surface of the Ga_2O_3 thin film PD during the AFM measurement, where the inset shows the simplified schematic illustration of a single PD device; (b) *I*–*V* characteristics of the Ga_2O_3 thin film PDs grown on sapphire, CeO_2, and p-Si substrates, where the solid circles represent the photocurrent under 250 nm illumination and the empty circles represent the corresponding dark current; (c) wavelength-dependent responsivity and (d) time-dependent photoresponse curves measured under 10 s on/off intervals of 250 nm illumination at a bias of 5 V of the Ga_2O_3 thin film PDs grown on sapphire, CeO_2, and p-Si substrates; (e) photocurrent response for one single cycle of the Ga_2O_3 thin film PDs grown on sapphire, CeO_2, and p-Si substrates; and (f) schematic of the Ga_2O_3 growth modes for sapphire, CeO_2, and Si substrates.

responsivity in the DUV region is slightly lower ($R_{nm}^{Si250} = 15\ A\ W^{-1}$); however, the photo-response spans to the visible-light region, yielding an ultra-low spectral selectivity ($R_{nm}^{Si250}/R_{nm}^{Si600} = 1.6$). The real-time transient photocurrent measurement was also measured on the three samples at a fixed bias of 5 V under a 250 nm illuminating light with a 10 s on/off interval for 200 s, as shown in Fig. 5(d). Again, the PD using the CeO_2 substrate shows a photocurrent and a dark current both similar to those using the sapphire substrate ($I_P^{Al_2O_3} \approx 0.25\ \mu A$, $I_D^{Al_2O_3} \approx 5$ nA; $I_P^{CeO_2} \approx 0.18\ \mu A$, $I_D^{CeO_2} \approx 5$ nA); however, the PD using the Si substrate shows a substantially lower photocurrent ($I_P^{Si} \approx 0.1\ \mu A$) and a higher dark current ($I_D^{Si} \approx 0.07\ \mu A$) in comparison with the other two samples. Additionally, the photocurrent response for one single cycle of the Ga_2O_3 thin-film PDs grown on the sapphire, CeO_2, and p-Si substrates are shown in Fig. 5(e), based on which the response time (τ_r) and the decay time (τ_d) for the samples are obtained by exponential fitting. Again, the PDs on sapphire and CeO_2 show similar response times (0.41 s for sapphire and 0.48 s for CeO_2) and decay times (0.7 s for sapphire and 0.78 s CeO_2 both), while the PD deposited on the p-Si substrate shows a response time and a decay time of 0.93 s and 455 s, respectively, manifesting a doubled response time and a decay time that is nearly three magnitudes higher in comparison with the other two samples.

In general, the results indicate that the photoelectrical performance of the β-Ga_2O_3 PD deposited on the CeO_2 substrate is similar to that on the conventional sapphire substrate and is significantly superior to that on the p-Si substrate. It is well known that on the sapphire substrate, the β-Ga_2O_3 thin films feature a single preferred orientation both in the *ab*-plane and out of the *ab*-plane (along the *c*-axis) due to the small lattice mismatch between sapphire (0001) and β-Ga_2O_3 (−201).[29,36–38] By contrast, as demonstrated by the pole-figure measurement (Fig. 4(a)), the CeO_2 substrate bestows a single preferred orientation along the *c*-axis but a dual-preferred orientation in the *ab*-plane (a 90° rotation angle between each other) on the growing β-Ga_2O_3 thin films. For the p-Si substrate, the $2\theta - \omega$ XRD data indicate that the β-Ga_2O_3 thin films are completely polycrystalline, that is, grown without out-of-plane orientation. Based on the XRD results, the growing modes of the β-Ga_2O_3 thin films on the sapphire, CeO_2, and p-Si substrates are shown in Fig. 5(f).

Compared with the PDs using the sapphire and CeO_2 substrates, the polycrystalline PD using the p-Si substrate has a large number of bulk defects and dangling bonds. They can influence the photoelectrical performance of the PD in two ways. First, upon illumination, the electrons are excited from the valence band to the conduction band. The trap states accumulated on the defects and dangling bonds can easily capture the excited electrons during their recombination. The associated ultra-slow desorption and adsorption processes at such trap states can dramatically decrease the photocurrent. Second, the highly populated defects and dangling bonds that are remnant in the polycrystalline structure can generate a large amount of intrinsic carriers, which is responsible for the observed high dark current and the high persistent photoconductivity.[31,39–41] Such a polycrystalline nature makes the PD sample using the p-Si substrate essentially different

from the other two highly oriented samples. More importantly, the PD sample using the CeO_2 substrate described in this research represents a photoelectrical performance very similar to that using the conventional sapphire substrate, both in terms of the high photocurrent, the low dark current, and the fast response and decay times. Compared with the conventional sapphire (0001) substrate, the β-Ga_2O_3 thin films gown on CeO_2 (001) can have a higher in-plane misorientation owing to the larger mismatch between the (−201) β-Ga_2O_3 and (001) CeO_2 planes and the two-domain formation in the (−201) β-Ga_2O_3 plane. However, the in-plane misorientation does not induce high structural disorder and dangling bonds, therefore the influence on the photoelectrical performance of the β-Ga_2O_3 PD is insignificant. Overall, the results suggest that the CeO_2 (001) substrate can readily serve as an appropriate epitaxial template for constructing (−201) β-Ga_2O_3/cubic functional layer heterostructures while largely maintaining the high photoelectrical performance of β-Ga_2O_3.

Conclusions

In conclusion, we demonstrate the epitaxial growth of β-Ga_2O_3 thin films on the CeO_2-coated YSZ substrate using the PLD technique. The $2\theta - \omega$ XRD spectra indicate the high phase purity of the deposited β-Ga_2O_3 thin films, without any by-product formation that is potentially induced by the diffusion of cerium from the CeO_2 layer to the Ga_2O_3 layer. All the grains are aligned along the [−201] direction. The rocking curve and the pole figure suggest the good out-of-plane and in-plane crystallization quality of the deposited β-Ga_2O_3 thin films. Interestingly, different from the conventional six-fold symmetric sapphire substrates, the four-fold symmetric cubic-phase CeO_2 induces the formation of two sets of hexagonal-like atom frameworks with a mutual phi-rotation angle of 90° in the β-Ga_2O_3 (−201) plane. This is due to the small lattice mismatch between the β-Ga_2O_3 (−201) plane and the CeO_2 (001) plane in two directions: CeO_2 [100]//β-Ga_2O_3 [010] and CeO_2 [010]//β-Ga_2O_3 [010]. The obtained epitaxial β-Ga_2O_3/CeO_2 thin films are fabricated into PDs and compared with those using sapphire and p-Si substrates. The key photoelectrical characteristics are found to be similar to the PDs based on epitaxial thin films using the conventional sapphire substrate and significantly superior to those based on polycrystalline thin films on the p-Si substrate. The results indicate that the epitaxial β-Ga_2O_3 thin films on CeO_2 have a high crystallization quality and thus are capable of producing various semiconductor devices.

Author contributions

Thin film growth and device fabrication were carried out by Xiao Tang, Che-Hao Liao, Kuang-Hui Li, and Shibin Krishna. AFM characterization was carried out by Jose Taboada and Na Xiao. TEM characterization was performed by Dongxing Zheng and Chen Liu. Silvaco Atlas TCAD simulation was done by Rongyu Lin. Administration and supervision of the project were carried out by Xiaohang Li. The writing of original draft was done by Xiao Tang and Xiaohang Li.

Conflicts of interest

There are no conflicts to declare.

Acknowledgements

The authors would like to thank the support of KAUST Baseline Funds BAS/1/1664-01-01, Competitive Research Grants URF/1/3437-01-01 and URF/1/3771-01-01, and GCC Research Council REP/1/3189-01-01.

References

1 D. Guo, Q. Guo, Z. Chen, Z. Wu, P. Li and W. Tang, Review of Ga_2O_3-based optoelectronic devices, *Mater. Today Phys.*, 2019, 11.
2 S. Rafique, L. Han, M. J. Tadjer, J. A. Freitas, N. A. Mahadik and H. Zhao, Homoepitaxial growth of β-Ga_2O_3 thin films by low pressure chemical vapor deposition, *Appl. Phys. Lett.*, 2016, **108**(18), 182105.
3 Z. Liu, Y. Zhi, S. Li, Y. Liu, X. Tang, Z. Yan, P. Li, X. Li, D. Guo, Z. Wu and W. Tang, Comparison of optoelectrical characteristics between Schottky and Ohmic contacts to β-Ga_2O_3 thin film, *J. Phys. D: Appl. Phys.*, 2020, **53**(8), 085105.
4 S. Nakagomi and Y. Kokubun, Crystal orientation of β-Ga_2O_3 thin films formed on *c*-plane and *a*-plane sapphire substrate, *J. Cryst. Growth*, 2012, **349**(1), 12–18.
5 M. Kneiß, A. Hassa, D. Splith, C. Sturm, H. von Wenckstern, T. Schultz, N. Koch, M. Lorenz and M. Grundmann, Tin-assisted heteroepitaxial PLD-growth of κ-Ga_2O_3 thin films with high crystalline quality, *APL Mater.*, 2019, **7**(2), 022516.
6 S. Nakagomi, T. Momo, S. Takahashi and Y. Kokubun, Deep ultraviolet photodiodes based on β-Ga_2O_3/SiC heterojunction, *Appl. Phys. Lett.*, 2013, **103**(7), 072105.
7 C. Caspers, A. Gloskovskii, W. Drube, C. M. Schneider and M. Müller, "Conductive" yttria-stabilized zirconia as an epitaxial template for oxide heterostructures, *J. Appl. Phys.*, 2014, **115**(17), 17c111.
8 X. Tang, Y. Zhao and J.-C. Grivel, Influence of initial pH on the microstructure of $YBa_2Cu_3O_{7-x}$ superconducting thin films derived from DEA-aqueous sol–gel method, *Ceram. Int.*, 2013, **39**(7), 7735–7741.
9 Q. Zou, M. Liu, G. Q. Wang, H. L. Lu, T. Z. Yang, H. M. Guo, C. R. Ma, X. Xu, M. H. Zhang, J. C. Jiang, E. I. Meletis, Y. Lin, H. J. Gao and C. L. Chen, Step terrace tuned anisotropic transport properties of highly epitaxial $LaBaCo_2O_{5.5}$ + delta thin films on vicinal $SrTiO_3$ substrates, *ACS Appl. Mater. Interfaces*, 2014, **6**(9), 6704–6708.
10 J. Shi, Y. Zhao, Y. Wu, J. Chu, X. Tang, X. Li, X. Yu, W. Wu, G. Jiang, H. Suo and Z. Jin, Pyrolysis behaviors dominated by the reaction–diffusion mechanism in the fluorine-free

metal–organic decomposition process, *J. Mater. Chem. C*, 2020, **8**(48), 17417–17428.

11 D. Zheng, J. Gong, C. Jin, P. Li and H. Bai, Crystal-Orientation-Modulated Exchange Bias in Orthorhombic-$YMnO_3/La_{0.6}Sr_{0.4}MnO_3$ Multiferroic Heterostructures, *ACS Appl. Mater. Interfaces*, 2015, **7**(27), 14758–14762.

12 Q. Y. Zhang, J. Shaibo, J. Ju, M. Liu, S. Cheng, Y. J. Ma, J. Y. Xiao, X. N. Jiang and C. Y. Ma, Rehabilitation of MgO(001) Substrate Surface for Growth of Single-Crystal $LaBaCo_2O_{5+\delta}$ Films by Magnetron Sputtering, *Cryst. Growth Des.*, 2016, **16**(8), 4272–4277.

13 R. Wakabayashi, K. Yoshimatsu, M. Hattori and A. Ohtomo, Epitaxial structure and electronic property of β-Ga_2O_3 films grown on MgO(100) substrates by pulsed-laser deposition, *Appl. Phys. Lett.*, 2017, **111**(16), 162101.

14 H. Nishinaka, D. Tahara and M. Yoshimoto, Heteroepitaxial growth of ε-Ga_2O_3 thin films on cubic (111)MgO and (111)yttria-stablized zirconia substrates by mist chemical vapor deposition, *Jpn. J. Appl. Phys.*, 2016, **55**(12), 1202BC.

15 K. Song, H. Zhang, H. Fu, C. Yang, R. Singh, Y. Zhao, H. Sun and S. Long, Normally-off AlN/β-Ga_2O_3 field-effect transistors using polarization-induced doping, *J. Phys. D: Appl. Phys.*, 2020, **53**(34), 345107.

16 J. Montes, C. Yang, H. Fu, T.-H. Yang, K. Fu, H. Chen, J. Zhou, X. Huang and Y. Zhao, Demonstration of mechanically exfoliated β-Ga_2O_3/GaN p–n heterojunction, *Appl. Phys. Lett.*, 2019, **114**(16), 162103.

17 D. Zheng, Y. W. Fang, S. Zhang, P. Li, Y. Wen, B. Fang, X. He, Y. Li, C. Zhang, W. Tong, W. Mi, H. Bai, H. N. Alshareef, Z. Q. Qiu and X. Zhang, Berry Phase Engineering in $SrRuO_3/SrIrO_3/SrTiO_3$ Superlattices Induced by Band Structure Reconstruction, *ACS Nano*, 2021, **15**(3), 5086–5095.

18 D. Majumder, I. Chakraborty, K. Mandal and S. Roy, Facet-Dependent Photodegradation of Methylene Blue Using Pristine CeO_2 Nanostructures, *ACS Omega*, 2019, **4**(2), 4243–4251.

19 Y. Zhao, J. M. Zhu, G. Y. Jiang, C. S. Chen, W. Wu, Z. W. Zhang, S. K. Chen, Y. M. Hong, Z. Y. Hong, Z. J. Jin and Y. Yamada, Progress in fabrication of second generation high temperature superconducting tape at Shanghai Superconductor Technology, *Supercond. Sci. Technol.*, 2019, **32**(4), 044004.

20 J. Chu, Y. Zhao, M. Z. Khan, X. Tang, W. Wu, J. Shi, Y. Wu, H. Huhtinen, H. Suo and Z. Jin, Insight into the Interfacial Nucleation and Competitive Growth of $YBa_2Cu_3O_{7-\delta}$ Films as High-Performance Coated Conductors by a Fluorine-Free Metal–Organic Decomposition Route, *Cryst. Growth Des.*, 2019, **19**(11), 6752–6762.

21 X. Tang, Y. Zhao, W. Wu, N. H. Andersen and J. C. Grivel, High-Jc $YBa_2Cu_3O_{7-x}$-Ag superconducting thin films synthesized through a fluorine-free MOD method, *J. Eur. Ceram. Soc.*, 2015, **35**(6), 1761–1769.

22 R. Yan, G. Khalsa, S. Vishwanath, Y. Han, J. Wright, S. Rouvimov, D. S. Katzer, N. Nepal, B. P. Downey, D. A. Muller, H. G. Xing, D. J. Meyer and D. Jena, GaN/NbN epitaxial semiconductor/superconductor heterostructures, *Nature*, 2018, **555**(7695), 183–189.

23 O. Brandt, H. Yang, H. Kostial and K. H. Ploog, High p-type conductivity in cubic GaN/GaAs(113)A by using Be as the acceptor and O as the codopant, *Appl. Phys. Lett.*, 1996, **69**(18), 2707–2709.

24 M. Falmbigl, I. S. Golovina, A. V. Plokhikh, D. Imbrenda, A. Podpirka, C. J. Hawley, G. Xiao, A. Gutierrez-Perez, I. A. Karateev, A. L. Vasiliev, T. C. Parker and J. E. Spanier, $BaTiO_3$ Thin Films from Atomic Layer Deposition: A Superlattice Approach, *J. Phys. Chem. C*, 2017, **121**(31), 16911–16920.

25 K. H. Li, N. Alfaraj, C. H. Kang, L. Braic, M. N. Hedhili, Z. Guo, T. K. Ng and B. S. Ooi, Deep-Ultraviolet Photodetection Using Single-Crystalline beta-Ga_2O_3/NiO Heterojunctions, *ACS Appl. Mater. Interfaces*, 2019, **11**(38), 35095–35104.

26 T.-G. Lee, H.-J. Lee, S.-W. Kim, D.-H. Kim, S. H. Han, H.-W. Kang, C.-Y. Kang and S. Nahm, Piezoelectric properties of $Pb(Zr,Ti)O_3$-$Pb(Ni,Nb)O_3$ ceramics and their application in energy harvesters, *J. Eur. Ceram. Soc.*, 2017, **37**(13), 3935–3942.

27 R. Mizutani, Y. Okamoto, H. Nagaso, Y. Yamakawa, H. Takatsu, H. Kageyama, S. Kittaka, Y. Kono, T. Sakakibara and K. Takenaka, Superconductivity in PtSbS with a Noncentrosymmetric Cubic Crystal Structure, *J. Phys. Soc. Jpn.*, 2019, **88**(9), 093709.

28 D. Szcześniak, A. Z. Kaczmarek, E. A. Drzazga, K. A. Szewczyk and R. Szcześniak, On the superconducting state in $Ba_{0.6}K_{0.4}BiO_3$ perovskite oxide, *Phys. Rev. B*, 2018, **536**, 676–681.

29 D. Guo, Z. Wu, P. Li, Y. An, H. Liu, X. Guo, H. Yan, G. Wang, C. Sun, L. Li and W. Tang, Fabrication of β-Ga_2O_3 thin films and solar-blind photodetectors by laser MBE technology, *Opt. Mater. Express*, 2014, **4**(5), 1067–1076.

30 X. C. Guo, N. H. Hao, D. Y. Guo, Z. P. Wu, Y. H. An, X. L. Chu, L. H. Li, P. G. Li, M. Lei and W. H. Tang, β-Ga_2O_3/p-Si heterojunction solar-blind ultraviolet photodetector with enhanced photoelectric responsivity, *J. Alloys Compd.*, 2016, **660**, 136–140.

31 D. Guo, H. Liu, P. Li, Z. Wu, S. Wang, C. Cui, C. Li and W. Tang, Zero-Power-Consumption Solar-Blind Photodetector Based on beta-Ga_2O_3/NSTO Heterojunction, *ACS Appl. Mater. Interfaces*, 2017, **9**(2), 1619–1628.

32 C.-H. Liao, K.-H. Li, C. G. Torres-Castanedo, G. Zhang and X. Li, Wide range tunable bandgap and composition β-phase $(AlGa)_2O_3$ thin film by thermal annealing, *Appl. Phys. Lett.*, 2021, **118**(3), 032103.

33 P. Song, Z. Wu, X. Shen, J. Kang, Z. Fang and T.-Y. Zhang, Self-consistent growth of single-crystalline (201)β-Ga_2O_3 nanowires using a flexible GaN seed nanocrystal, *CrystEngComm*, 2017, **19**(4), 625–631.

34 W. Seiler, M. Selmane, K. Abdelouhadi and J. Perrière, Epitaxial growth of gallium oxide films on c-cut sapphire substrate, *Thin Solid Films*, 2015, **589**, 556–562.

35 W. Li, X. Zhang, R. Meng, J. Yan, J. Wang, J. Li and T. Wei, Epitaxy of III-Nitrides on beta-Ga_2O_3 and Its Vertical Structure LEDs, *Micromachines*, 2019, **10**(5), 322.

36 Y. Li and W. Shen, Morphology-dependent nanocatalysts: rod-shaped oxides, *Chem. Soc. Rev.*, 2014, **43**(5), 1543–1574.
37 D. Y. Guo, Z. P. Wu, Y. H. An, X. C. Guo, X. L. Chu, C. L. Sun, L. H. Li, P. G. Li and W. H. Tang, Oxygen vacancy tuned Ohmic-Schottky conversion for enhanced performance in β-Ga_2O_3 solar-blind ultraviolet photodetectors, *Appl. Phys. Lett.*, 2014, **105**(2), 023507.
38 S. Rafique, L. Han, A. T. Neal, S. Mou, J. Boeckl and H. Zhao, Towards High-Mobility Heteroepitaxial β-Ga_2O_3 on Sapphire – Dependence on The Substrate Off-Axis Angle, *Phys. Status Solidi A*, 2018, **215**(2), 1700467.
39 K. Arora and M. Kumar, Sputtered-Growth of High-Temperature Seed-Layer Assisted β-Ga_2O_3 Thin Film on Silicon-Substrate for Cost-Effective Solar-Blind Photodetector Application, *ECS J. Solid State Sci. Technol.*, 2020, **9**(6), 065013.
40 H. Liang, S. Cui, R. Su, P. Guan, Y. He, L. Yang, L. Chen, Y. Zhang, Z. Mei and X. Du, Flexible X-ray Detectors Based on Amorphous Ga_2O_3 Thin Films, *ACS Photonics*, 2018, **6**(2), 351–359.
41 B. Zhao, F. Wang, H. Chen, L. Zheng, L. Su, D. Zhao and X. Fang, An Ultrahigh Responsivity (9.7 mA W^{-1}) Self-Powered Solar-Blind Photodetector Based on Individual ZnO–Ga_2O_3 Heterostructures, *Adv. Funct. Mater.*, 2017, **27**(17), 1700264.

